Hybrid Method for Determining the Fraction of Plastic Work Converted to Heat

by A. T. Zehnder, E. Babinsky and T. Palmer

ABSTRACT—The fraction of plastic work converted to heat is typically measured either by nearly isothermal experiments, in which the thermal energy is measured during a deformation experiment with a calorimeter, or by adiabatic experiments, in which the thermal energy is determined from the temperature rise, measured either during the test or immediately after the test by dropping the sample into a calorimeter. In the present work, the temperature is measured with a single fine-wire thermocouple. The restriction to adiabatic loadings is relaxed by using a hybrid method that combines the measurements with finite difference simulations to calculate the heat losses that occur during the test. These heat losses are then accounted for in the final energy balance to determine the fraction of plastic work converted to heat. The method is applied to annealed 302 stainless steel. The results show that the fraction of plastic work converted to heat is a decreasing function ranging from 0.7 to 0.4 over a tensile strain range of 0 to 0.15. An analysis of the restrictions to this method and of the potential errors is given.

Introduction

It has long been known that the work of plastic deformation in metals is largely dissipated as thermal energy with the balance stored in the material as defect energy and as residual strain energy due to incompatible slip. It is said that Tresca (ca. 1870) was the first to notice and record heating due to plastic deformation,[1] although surely the Romans and our other ancient predecessors noticed the same phenomena when they hammered out coins, weapons and other products. The modern study of thermomechanics originated with the work of Taylor, Farren and Quinney, who, in 1925 and 1934, published measurements of the heat generated during the plastic deformation of various metals.[2,3] Since then, many further experiments have been performed,[4] mostly from the perspective of materials scientists who are interested not in the energy dissipated but in the energy stored and its effects on recrystallization of the material. In mechanics, interest in the dissipation of energy is due to the heating produced during rapid deformations such as shear banding, penetration and cutting. Temperature increases in such deformations lead to thermal softening of the material, promoting further deformation and more heating, and potentially leading to runaway deformation, as occurs in adiabatic shear bands.

Let us define the fraction of plastic work dissipated as thermal energy to be

$$\beta \equiv \frac{\dot{Q}}{\dot{W}^p}, \tag{1}$$

where $\dot{Q}$ is the thermal dissipation rate and $\dot{W}^p$ is the plastic work rate. For many years, Taylor and Quinney's result that $\beta \approx 0.90$ sufficed for analyses. However, ever-increasing sophistication of numerical modeling of dynamic deformations requires better constitutive information, including better information on β. In addition, reliable measurements of β, particularly as a function of plastic strain and plastic strain rate, are valuable in helping to formulate and validate micromechanically based models of deformation that seek to predict β.[5–7]

Measurements of β can be classified into single-step and two-step methods.[4] In single-step methods, the heat of plastic deformation is measured either during the deformation or immediately after, using a calorimeter. In two-step methods, the material is deformed, and the stored energy is measured later. The single-step methods are typically either nearly adiabatic or isothermal. The original works by Taylor, Farren and Quinney were examples of nearly adiabatic deformations. In these experiments, the samples were rapidly loaded and either the temperature rise was recorded during the loading or the sample was placed in a calorimeter immediately following the loading. By means of several calibration measurements, these authors were able to determine that the heat loss during these tests was negligible, and thus the results could be analyzed assuming an adiabatic process.

A more recent example of a truly adiabatic experiment is the work of Mason, Rosakis and Ravichandran,[8] who measured β for aluminum, steel and titanium alloys by loading the samples in a Kolsky bar at strain rates on the order of 1000/s, and measuring the resulting temperature rise using InSb infrared detectors. In this case, the total duration of the experiment is less than 1 ms and the process is truly adiabatic. This approach suffers from a lack of absolute accuracy in the temperature measurement due to a limited signal-to-noise ratio of infrared detectors and uncertainties associated with their calibration. Nonetheless, it remains the only demonstrated approach capable of estimating β at high strain rates.

Note that due to the relatively slow rate of temperature propagation in solids, the loading rate could have been much slower (by 1000 times) than the experiments of Mason, Rosakis and Ravichandran and still have been adiabatic.

A.T. Zehnder (SEM Member) is Associate Professor, Department of Theoretical and Applied Mechanics, and E. Babinsky and T. Palmer are Undergraduate Research Assistants, Cornell University, Ithaca, NY 14853.

Original manuscript submitted: January 2, 1998.
Final manuscript received: August 10, 1998.

To estimate the time span over which a deformation is adiabatic, one can use the Fourier number

$$F_0 \equiv \frac{\alpha t}{l^2}, \tag{2}$$

where α is the thermal diffusivity, t is the time and l is a characteristic sample dimension. When $F_0 < 0.01$ (short times), the process is essentially adiabatic. When $F_0 > 10$, the process is essentially isothermal. For a metal, a typical value is $\alpha = 10^{-5} m^2/s$. If $l = 0.01m$, then if $t < 0.1s$, the process is adiabatic.

It is in a range intermediate to adiabatic and isothermal—that is, $0.01 < F_0 < 10$—that the current experiments are performed. Thermocouples can be used to measure the temperature rise by slowing down the loading relative to the Kolsky bar type tests. This has the advantage of high absolute accuracy, since thermocouple calibrations are NIST traceable. A disadvantage is the limited strain rate that can be used due to the finite response time of even the smallest thermocouple junctions. By using finite difference simulations to account for the conduction, convection and radiation heat losses that occur during the test, temperature rise measurements from experiments that are not truly adiabatic can be used to determine β as a function of plastic strain. Similar approaches were taken by Beghi *et al.*,[9] who used the temperature of the specimen measured at several locations to estimate the conductive heat flux, and by Wong and Kirby,[10] who used measured temperatures in conjunction with finite difference simulations to estimate the heat flux and hence β during low-cycle fatigue of an aluminum alloy.

Experimental Method and Apparatus

The experiments were performed using dogbone tensile specimens punched from sheets of vacuum-annealed 302 stainless steel, with the dimensions shown in Fig. 1. The mechanical and thermal properties of the material are given in Table 1. The samples were loaded in tension in an Instron 1320 testing machine at cross-head speeds of 50, 78 and 90 mm/min, corresponding to strain rates of 0.038, 0.06 and 0.068 1/s, respectively. The temperature of the specimen was measured by taping a type E thermocouple made from 0.025-mm (0.001-in.) diameter wires directly to the surface of the sample. These thermocouples were chosen as a compromise between fast response time and ease of handling. Even finer (0.0123-mm diameter) wires were tried, but without success due to their frailty. The time response of the 0.025-mm diameter wires when immersed in water is on the order of 0.002 s, and on the order of 0.05 s when immersed in air.[11] When a thermocouple is in contact with the surface of the 302 stainless steel specimen, the effective response time will be intermediate to the response times in water and air. The loading duration of our experiments is on the order of one second, so even if the response time is closer to the response time in air, the thermocouples are still fast enough for our work. One side of the thermocouple junction is in contact with the sample, and the other side is in contact with a polymer tape. By making the tape of a relatively low-conductivity material, such as a polymer, the heat conduction from the thermocouple to the tape is minimized, keeping the thermocouple at the same temperature as the metal surface.

Load, displacement (measured using an LVDT) and temperature were sampled and recorded at a rate of 100 points per second using a 12-bit digital oscilloscope (Nicolet 440). The data were then transferred to a computer system for analysis. Examples of the recorded data are given in Figs. 2 and 3, which plot the temperature rise and true stress as functions of time for two cross-head displacement rates. True stress is computed from the load using the assumption of plastic incompressibility. Note the small temperature drop at the start of the test due to the thermoelastic effect. The temperature starts to drop after the sample breaks (the stress drops to zero). The rate of cooling after sample break was used to help validate the thermal analysis.

TABLE 1—MATERIAL PROPERTIES OF ANNEALED 302 STAINLESS STEEL

Thermal diffusivity (α)	3.93×10^{-6} m^{2}s
Thermal conductivity (k)	15.7 W/m· K
Average emissivity ($\bar{\varepsilon}$)	0.59
Coefficient of thermal expansion (a_{cte})	17.3×10^{-6}/K
Specific heat (c)	500 J/kg · K
Density (ρ)	8,000 kg/m^3
Modulus of elasticity (E)	193 GPa
Yield stress	380 MPa

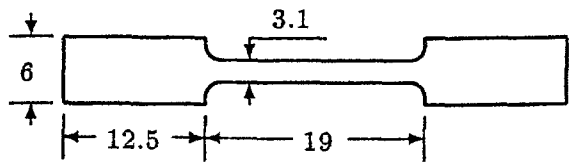

Fig. 1—Dogbone tension test sample of annealed 302 stainless steel, 0.10 mm thick. All dimensions are in mm

Theory and Analysis

Thermomechanics Theory

The plastic work rate per unit volume (assuming homogeneous deformation and uniaxial loading) is

$$\dot{W}^p = \sigma \dot{\varepsilon}^p, \tag{3}$$

where $\dot{W}^p$ is the plastic work rate, σ is the stress and $\dot{\varepsilon}^p$ is the plastic strain rate,

$$\dot{\varepsilon}^p = \dot{\varepsilon} - \dot{\sigma}/E, \tag{4}$$

where $\dot{\varepsilon}$ is the total strain rate and E is the modulus of elasticity.

Let us at first neglect heat transfer. Then, the energy balance is

$$\underbrace{\dot{W}^p_{in}}_{\text{plastic work in}} = \sigma\left[\dot{\varepsilon} - \frac{\dot{\sigma}}{E}\right] = \underbrace{\rho c \dot{T}}_{\text{thermal energy stored}} + \underbrace{\dot{W}_s}_{\text{work stored}}. \tag{5}$$

If *heat transfer is neglected*, the expression for β becomes

$$\beta = \frac{\rho c \dot{T}}{\dot{W}^p} = \frac{\rho c \dot{T}}{\sigma[\dot{\varepsilon} - \dot{\sigma}/E]}. \tag{6}$$

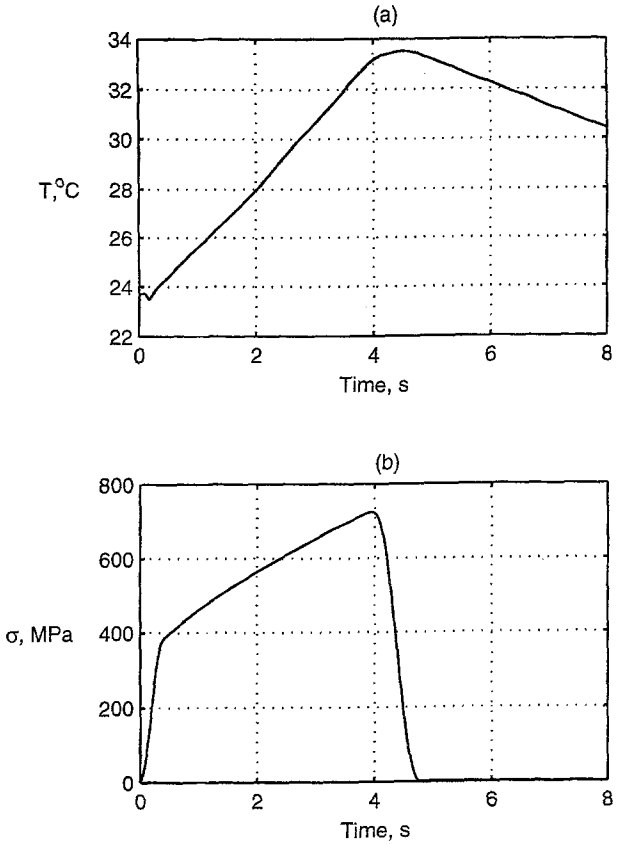

Fig. 2—Temperature and true stress as a function of time for 50-mm/min stretching rate

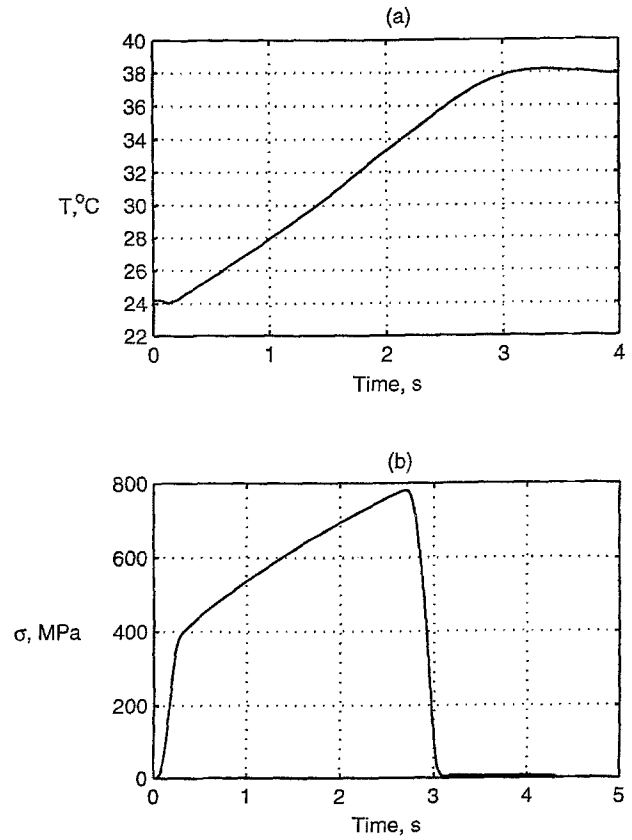

Fig. 3—Temperature and true stress as a function of time for 90-mm/min stretching rate

Since the present experiment is carried out at low strain rates, heat transfer must be considered. As shown in Fig. 4, the specimen is modeled as a flat plate insulated on the sides, and one-dimensional heat flow (along the plate) is assumed; that is, $T = T(x, t)$ only. The specimen loses energy by conduction into the grips and by convection and radiation from the top and bottom surfaces. An energy balance is performed on a differential element of the specimen to obtain the governing heat transfer equation

$$\dot{T} = \alpha T_{,xx} - \frac{2\alpha(t+w)}{Ak}\left[h(T - T_\infty) + \bar{\sigma}\bar{\varepsilon}(T^4 - T_\infty^4)\right] + \frac{\alpha}{k}\dot{q}, \tag{7}$$

where w is the plate width, t is the plate thickness, A is the cross-sectional area of the plate, k is the conductivity, $\bar{\sigma}$ is the Stefan-Boltzmann constant, $\bar{\varepsilon}$ is the average emissivity of the surface, h is the convective heat transfer coefficient, T is the absolute temperature and T_∞ is the absolute ambient temperature. The heat generation term, $\dot{q}$, consists of two effects: heating due to plastic work and cooling due to the thermoelastic effect.[12] Assuming homogeneous deformation and uniaxial loading, the heat generation term can be expressed as

$$\dot{q} = \beta \dot{W}^p - \dot{\alpha} a_{cte} T_\infty, \tag{8}$$

where a_{cte} is the coefficient of thermal expansion. The convection coefficient is computed using an empirical correlation for natural convection from an isothermal vertical plate[13]

$$\log_{10}(Nu) = -6.2 \times 10^{-4} Ra^3 + 1.9 \times 10^{-2} Ra^2 + 8.2 \times 10^{-2} Ra + 1.9 \times 10^{-1} \tag{9}$$

$$Nu = \frac{hl}{k_f} \quad Gr = \frac{g\bar{\beta}(T - T_\infty)l^3}{\nu^2} \quad Ra = GrPr,$$

where Nu is the Nusselt number, Gr is the Grashof number, Ra is the Rayleigh number, $Pr = \nu/\alpha$ is the Prandtl number, l is the characteristic length of the specimen, k_f is the thermal conductivity of air, g is the gravitational acceleration, $\bar{\beta}$ is the volume coefficient of expansion of air, ν is the kinematic viscosity of air, α is the thermal diffusivity of air and h is the convection coefficient. The correlation is valid for Rayleigh numbers from 10^{-1} to 10^4. The length of the plate is the length scale used in the correlation. The heat transfer coefficient from an isothermal horizontal plate is approximately half of that from an isothermal vertical plate.

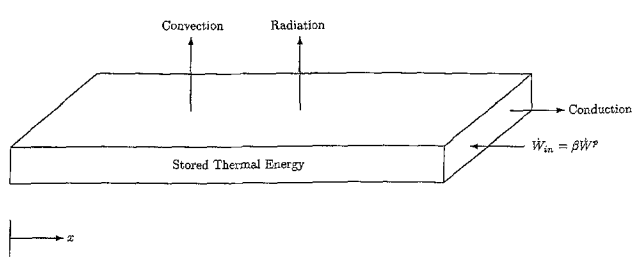

Fig. 4—Energy balance for deriving heat conduction equation. Edges of the sample are assumed to be insulated

Mollification of Temperature Data

The dependence of β on plastic strain is calculated by iteratively solving the inverse problem: given the temperature history, determine the value of β for which the temperature predicted by the governing equation matches the measured temperature. This requires computing the time derivative of the experimental temperature history, which presents some difficulties, since any empirical data invariably contain some noise. The data can be decomposed into two parts: the "signal" function that would be obtained in the absence of error and noise and the "noise" function

$$f(t)_{data} = s(t)_{signal} + n(t)_{noise}. \tag{10}$$

The process of differentiation is such that small errors in the data function $f(t)$ might produce large errors in the derivative function, regardless of how smooth the error function $n(t)$ is.[14] For example, consider a situation in which the noise is a very smooth function of t

$$n(t) = \frac{1}{\alpha}\sin(\alpha^2 t) \tag{11}$$

$$n'(t) = \alpha\cos(\alpha^2 t). \tag{12}$$

By selecting a large α, the noise in the original function can be made arbitrarily small, whereas the error in the derivative can be made arbitrarily large. This is illustrated further in Fig. 5—the signal-to-noise ratio of the data (see Figs. 2 and 3) is approximately 100:1; yet, the derivative is highly erratic.

To obtain a derivative of a noisy function that approximates the derivative of the signal function, the noisy function must be stabilized, or "smoothed." That is, the data function $f(t)$ must be transformed into a different, differentiable function $f_m(t)$ so that $f_m'(t) = f'(t) + \epsilon$, where ϵ is some arbitrary error level. The mollification method offers a way of obtaining $f_m(t)$.[14]

The mollification method requires the selection of a "blurring" function; for example, the Gaussian kernel of blurring radius δ:

$$\rho_\delta(t) = \frac{1}{\delta\sqrt{\pi}}\exp\left(-\frac{t^2}{\delta^2}\right). \tag{13}$$

The Gaussian kernel has three important properties: it falls off to zero within three blurring radii, it is infinitely differentiable and it has total integral of one.

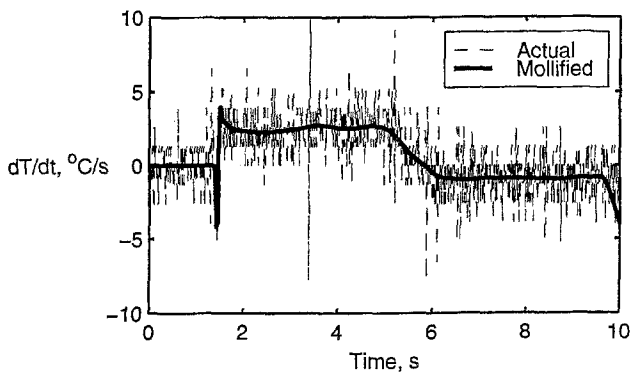

Fig. 5—Time derivative of temperature before and after mollification

The noisy data function (defined on [0, 1]) is extended to $[-\infty, \infty]$ in such a way that it decays smoothly to zero in $[-3\delta, 1 + 3\delta]$. The extension can be accomplished by defining[14]

$$f(t) = f(0)\exp\left\{\frac{t^2}{(3\delta)^2 - t^2}\right\} \qquad -3\delta \le t \le 0 \tag{14}$$

$$f(t) = f(0)\exp\left\{\frac{(t-1)^2}{[(t-1)^2 - (3\delta)^2]}\right\} \qquad 1 \le t \le 1 + 3\delta. \tag{15}$$

The mollified function is obtained by convolving the extended noisy data function with the Gaussian kernel. Essentially, the mollification process constructs the smoothed function by taking a weighted average of the data points in the vicinity of the point of interest (the size of the "vicinity" is determined by the blurring radius):

$$f_m(t) = (\rho_\delta * f)(t) = \int_{-\infty}^{\infty} \rho_\delta(t-s)f(s)\,ds = \int_{t-3\delta}^{t+3\delta} \rho_\delta(t-s)f(s)\,ds. \tag{16}$$

The derivative of the noisy function can be obtained either by

$$f_m(t)' = (\rho_\delta * f)'(t) = (\rho_\delta * f')(t) = (\rho_\delta' * f)(t) \tag{17}$$

or by differentiating the mollified function directly.

The construction of the derivative of the mollified function is a stable problem (small errors in the mollified function will not cause gross errors in the derivative function). In addition, the mollification process is monotonic with respect to the blurring radius δ, which implies that there exists a unique δ such that the norm of the difference between the mollified function and the original function is equal to the noise level; this is defined as the optimal blurring radius.

The blurring radius is used to control the mollification process. A large δ results in a very smooth mollified function at the expense of producing a derivative that deviates substantially from the true derivative. Several methods for determining the optimum radius of mollification have been suggested;[15,16] however, using the optimum δ does not automatically guarantee that the norm of the difference between the mollified function and the original function is within a specified tolerance. Occasionally, it is advantageous to use a smaller-than-optimal δ to ensure that the mollified function follows the original function more closely. For our data, the blurring radius was typically 5-10 percent of the domain of a given function.

Finite Difference Solution of Heat Transfer Problem

The governing heat transfer problem [eq (7)] is solved numerically using the forward time, centered space (FTCS) algorithm. The temporal and spatial steps are selected so that the algorithm is of order $O(\Delta x^2)$ in space and of order $O(\Delta t^4)$ in time.[17] The boundary condition $T = T_\infty$ is imposed at both ends of the specimen because the thermal mass

of the grips of the testing machine is very large. The spatial domain becomes progressively larger over time to account for the extension of the specimen. The convection coefficient is temperature dependent; however, constant average emissivity is assumed.

The calculation proceeds as follows: (1) the spatial distribution of temperature at time $t + dt$ is computed using an arbitrary value of β; (2) the temperature at the center of the specimen is compared with the experimental temperature—β is adjusted (using the bisection method), and the temperature is recalculated until the difference between the two temperatures is less than a specified tolerance; (3) after the value of β is obtained from step (2), the spatial distribution at time $t + dt$ is adjusted so that the temperature at the center of the specimen is equal to the experimentally measured temperature; (4) the next time step is taken using (3) as the initial condition. This procedure ensures that errors are not accumulated as the equation is integrated.

Results and Discussion

An excellent way to check the accuracy of the numerical calculation is to compare the calculated cooling rates to the experimental ones. A modified numerical procedure is used to accomplish this. The usual calculation is performed until the time when the specimen fractures; temperature matching is turned off thereafter. Figure 6 shows that when all of the heat losses are accounted for, the difference between the calculated and the experimental cooling rate is less than 10 percent, which is well within the range of experimental error. The graph also demonstrates the relative importance of considering various modes of heat transfer: radiation accounts for approximately 20 percent of the difference between cooling rates, and conduction and convection account for 40 percent each.

In separate tests, the same dogbone samples were deformed in tension and the temperature field over the entire specimen was measured using an infrared camera. Uncertainties with the calibration of the sample's emissivity make the use of the data for quantitative analysis difficult; however, we can use the results to show that the heat transfer analysis is essentially correct. Figure 7 compares the shape of the calculated spatial distribution to that from infrared data. The spatial distribution is computed numerically, and the temperature is matched to the infrared data at the center of the specimen at $t = 2.5$ s. The results of Fig. 7 show that the calculated distribution is essentially identical to the experimental one, lending confidence to the accuracy of the heat transfer calculations.

Over the limited strain range of these experiments, the material response is rate independent. This can be seen clearly in Fig. 8, which plots the true stress-true (logarithmic) strain curves for the 50- and 90-mm/min loading rates. The two curves lie directly on top of each other. There is no significance to the higher strain to failure at 90 mm/min. This is simply a reflection of random defects in the test specimens.

Using the procedures discussed above, $\beta(\varepsilon^p)$ was determined for each of four tests, two at loading rates of 50 mm/min, one at 78 mm/min, and one at 90 mm/min. To show the effect of accounting for heat loss, $\beta(\varepsilon^p)$ is shown in Fig. 9, calculated assuming adiabatic conditions and accounting for heat loss. At the lower loading rate, the difference between the actual and adiabatic β is approximately 16 percent. At the higher loading rate, the difference is closer to 8 percent, since for a faster test the process is closer to being adiabatic. Figure 9 also shows that the values of β from tests conducted at different strain rates lie in the same broad region of 0.7 to 0.3. This suggests that β is strain rate independent over the limited range of these experiments. This is consistent with

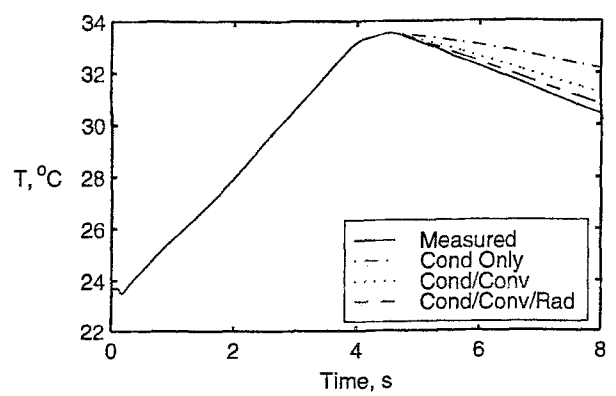

Fig. 6—Temperature versus time for a 50-mm/min stretching rate test. The measured data are shown along with simulated data accounting only for conduction, for conduction and convection, and for conduction, convection and radiation

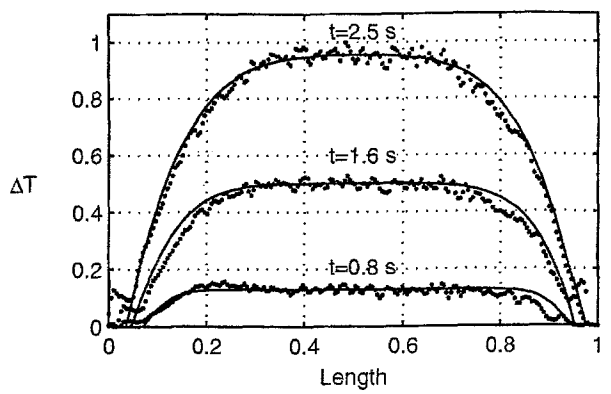

Fig. 7—Temperature profile along the length of the specimen. Temperature is normalized by its value at 2.5 s. Length is normalized by sample length. The dotted lines are from measurements performed using an infrared camera, and the solid lines are from the simulation

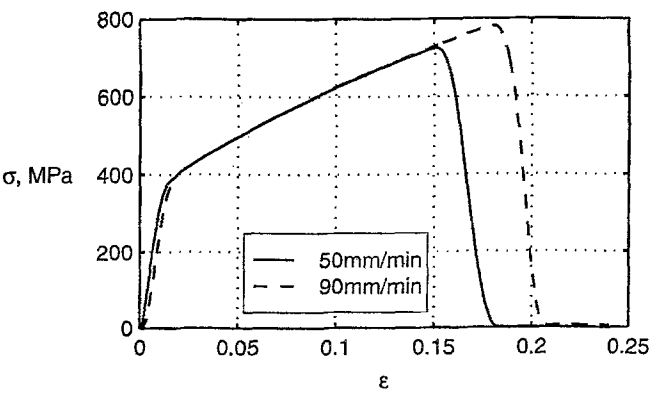

Fig. 8—True stress-strain for the 50- and 90-mm/min stretching rates

the stress-strain curves (Fig. 8), which also do not depend on the strain rate.

Assuming that β is independent of strain rate, a "composite" $\beta(\varepsilon^p)$ was determined by taking the average from the four tests at three different strain rates. The result, given in Fig. 10, shows that β is a decreasing function of plastic strain, ranging from 0.7 at zero strain to 0.4 at $\varepsilon^p = 0.15$.

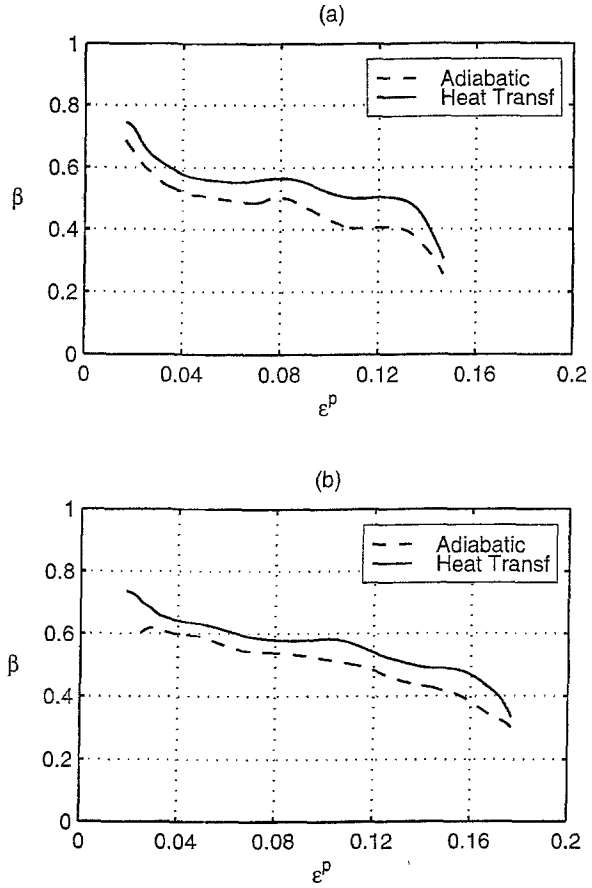

Fig. 9—The fraction of plastic work converted to heat, β for (a) 50-mm/min stretching, (b) 90-mm/min stretching. The dashed line gives the value of β one would get assuming adiabatic conditions. The solid line gives the true value, corrected for heat losses

To get some idea of the test-to-test variation and of the uncertainty in β, the β values from all four tests are plotted together in Fig. 11. The maximum difference in β is approximately 20 percent; thus, we can estimate the uncertainty of the $\beta(\varepsilon^p)$ curve in Fig. 10 to be approximately ±10 percent. The uncertainty in β is less than the change in β, indicating that β is indeed decreasing with ε^p.

Figure 8 shows that the material has nearly linear hardening but is slightly concave down. The simple dislocation-based theories for β[5,6] would predict that β increases slightly with ε^p. This is clearly not the case, since β decreases. A decreasing β is consistent with the model of Aravas, Kim and Leckie,[7] which gives an upper bound to β based on stored energy of incompatible deformations. Applying their model to the stress-strain curves in Fig. 8 yields $\beta = 0.7$ at $\epsilon^p = 0.05$ and $\beta = 0.65$ at $\epsilon^p = 0.15$. Both of these are higher than the measured values of β consistent with the result that the model gives upper bounds to β.

Applicability and Recommended Parameters of the Hybrid Method

Within limits, the hybrid method discussed here can be used over a broad range of strain rates and geometric configurations of the specimens. If the strain rate used is too high, the thermocouple response time becomes inadequate and the resulting lag affects the accuracy of the results. On the other hand, if the strain rate is too low, very low temperature rises occur and uncertainties in heat transfer parameters introduce very large uncertainties in the result. To determine the range of applicability of the hybrid method, numerical sensitivity analyses were performed.

If eq (7) is nondimensionalized, the following equation is obtained:

$$\dot{\theta} = \theta_{,\xi\xi} - \frac{2Bi}{\eta^2}(\theta - 1) + \frac{\alpha}{k}\hat{\dot{q}}, \tag{18}$$

where $\theta = T/T_\infty$, $\dot{\theta} = \partial\theta/\partial F_0$, $F_0 = \alpha t/l^2$, $Bi_h = ht/k$, $\hat{q} = q/T_\infty$, F_0 is the Fourier number, Bi is the Biot number, t is the thickness of the specimen, l is the length of the specimen, h is the effective average convection coefficient, k is the conductivity, $\eta = t/l$, ξ is the nondimensional position.

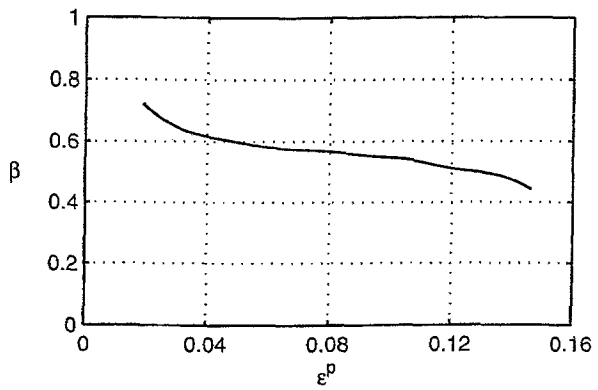

Fig. 10—Composite β versus plastic strain, obtained by averaging the β versus plastic strain results from all tests

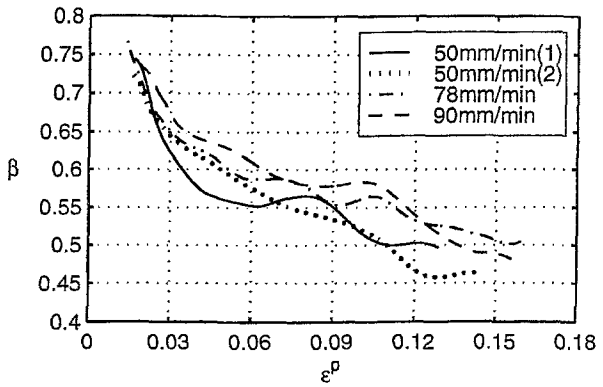

Fig. 11—Values of β for four tests to show spread in the data

Hence,

$$T = T_\infty \cdot \theta = T_\infty \cdot \theta\left(F_0,\ \xi,\ Bi/\eta^2,\ \frac{\alpha}{k}\dot{\hat{q}}\right). \qquad (19)$$

Thus, temperature is a function of nondimensional time, nondimensional position along the length of the specimen, the ratio Bi/η^2 and nondimensional energy input rate. If we neglect the dependence of temperature on the energy input rate and consider a fixed value of position (e.g., the middle of the specimen), the general relationship above reduces to

$$T = T_\infty \cdot \theta(F_0, Bi/\eta^2), \qquad (20)$$

where the Fourier number is based on the duration of the experiment and the Biot number is based on the thickness of the specimen and on the average effective convection coefficient.

The greatest uncertainty in the numerical simulation is due to uncertainty in the emissivity and the convection coefficient. In the worst possible case, uncertainty in either of these quantities should not exceed 25 percent. This error limit is used in the sensitivity analysis.

The sensitivity analysis proceeds as follows: (1) the temperature history is computed using the load data and composite β obtained from the dogbone experiments; (2) heat transfer is increased by 25 percent, and the temperature history is recalculated. The sensitivity analysis is carried out either at a fixed F_0 or at a fixed Bi/η^2. The difference between the two results is reported as the error norm, which is computed as follows:

$$\text{Error norm} = \frac{\int_0^{t_{\max}} |T_0^2 - T_{25\%}^2|^{\frac{1}{2}}\, dt}{\int_0^{t_{\max}} T_0\, dt}, \qquad (21)$$

where T_0 is the midpoint temperature history computed in step (1) above and $T_{25\%}$ is the midpoint temperature history computed in step (2) above.

The results of the sensitivity analysis are presented in Fig. 12. In the present experiment, the fastest and the slowest speeds correspond to Fourier numbers of 0.02 and 0.04, respectively, and Bi/η^2 of 1.4. From Fig. 12, the uncertainty in the present experiment due to possible errors in the heat transfer parameters is estimated to be approximately 6 percent for the 50-mm/min test and approximately 4 percent for the 90-mm/min test.

To ensure that the overall error remains under 10 percent, the hybrid method should be used under the following conditions:

$$\begin{aligned} F_0 &\le 0.1 \\ Bi/\eta^2 &\le 2.5. \end{aligned} \qquad (22)$$

The Fourier number restricts the duration of the test, whereas the Biot number restricts the thickness of the specimen. If the specimen is too thin (large Bi/η^2) or the test takes too long (large F_0), the heat losses result in a low temperature rise and, hence, produce a large error.

On the other hand, if the specimen is too thick (small Bi/η^2), a one-dimensional heat conduction calculation is no longer a good approximation. In this case, a two-dimensional analysis must be performed. In addition, if the Fourier number is too small, large errors in measured temperature will result because of thermocouple lag. These two conditions introduce additional restrictions on the range of F_0 and Bi/η^2; hence, F_0 should be greater than 0.02 for the diameter of thermocouples used in the present experiment, and Bi/η^2 should be greater than 0.5.

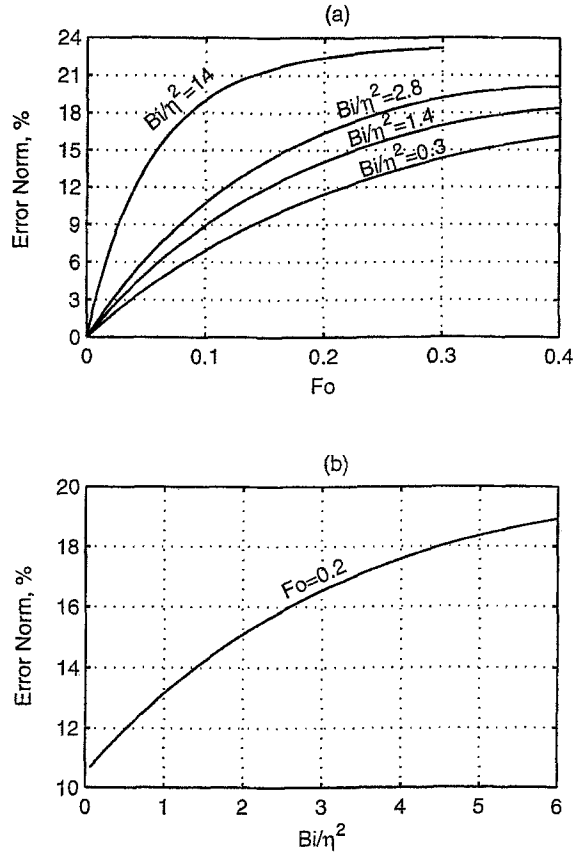

Fig. 12—Error estimates and sensitivity analysis for various stretching rates and thicknesses of the specimen. Twenty-five percent error in heat transfer parameters was assumed

Summary and Conclusions

A hybrid experimental-numerical procedure was developed and tested for determining the fraction of plastic work converted to heat from temperature measurements during loadings that are not adiabatic. Even though the heat transfer analysis performed in the present experiments is limited to one-dimensional heat conduction in flat plates, the hybrid method can be modified to handle heat transfer in 2-D and 3-D and in specimens of various geometries. The method was applied to annealed 302 stainless steel. The results show that β is a decreasing function of strain, ranging from $\beta = 0.7$ at $\varepsilon^p = 0$ to $\beta = 0.4$ at $\varepsilon^p = 0.15$. Guidelines for applying the procedure were established, and they show that the hybrid method can be used when the test duration is such that $F_0 \le 0.1$ and when the sample is thick enough to satisfy $Bi/\eta^2 \le 2.5$.

Acknowledgments

This work was supported by the National Science Foundation through two REU programs, Award EEC-9300579 made to the Department of Theoretical and Applied Mechanics,

and the program run by the Cornell Center for Materials Research (CCMR), Award DMR-9632275. The experiments were carried out in the Mechanical Testing Facility and the computations in the Multi-User Computational Facility, both run by the CCMR. The first author is indebted to Profs. Robert Thomas and Skip Favro of Wayne State University for hosting him for a week at Wayne State in 1996 and making their high speed infrared camera available. The data in Fig. 7 are a result of that work.

References

1. Bell, J., The Experimental Foundations of Solid Mechanics, Springer-Verlag, New York (1973).

2. Farren, W.S. and Taylor, G.I., "The Heat Developed During Plastic Extension of Metals," Proc. Roy. Soc., Series A, **107**, *422–451 (1925).*

3. Taylor, G.I. and Quinney, M.A., "The Latent Heat Remaining in a Metal After Cold Work," Proc. Roy. Soc., Series A, **143**, *307–326 (1934).*

4. Bever, M.B., Holt, D.L., and Titchener, A.L., "The Stored Energy of Cold Work," Prog. Mat. Sci., **17** *(1973).*

5. Nabarro, F.R.N., Theory of Crystal Dislocations, Dover, New York (1987).

6. Zehnder, A.T., "A Model for the Heating Due to Plastic Work," Mechanics Research Communications, **18**, *23–28 (1991).*

7. Aravas, N., Kim, K.S., and Leckie, F.A., "On the Calculations of the Stored Energy of Cold Work," J. Eng. Mat. Tech., **112**, *465–475 (1990).*

8. Mason, J.J., Rosakis, A.J., and Ravichandran, G., "On the Strain and Strain-rate Dependence of the Fraction of Plastic Work Converted to Heat: An Experimental Study Using High Speed Infrared Detectors and the Kolsky Bar," Mech. Mat., **17**, *135–145 (1994).*

9. Beghi, M.G., Bottani, C.E., Caglioti, G., and Lenti, A., "Energy Balance via Thermal Emission in Copper Under Stress," Mat. Lett., **6**, *133–137 (1988).*

10. Wong, A.K. and Kirby, G.C. III, "Determination of the Heat Dissipated from a Specimen Undergoing Cyclic Plasticity by a Hybrid Numerical/Experimental Method," NRL Memorandum Report 6633 (1990).

11. Omega Corporation, The Temperature Handbook (1997).

12. Carlson, D.E., "Linear Thermoelasticity," Encyclopedia of Physics, **VIa/2**, *Mechanics of Solids II, ed. C. Truesdell, Springer-Verlag, New York, 297–345 (1972).*

13. Holman, J.P., Heat Transfer, 8th ed., McGraw-Hill, New York (1997).

14. Murio, D.A., The Mollification Method and the Numerical Solution of Ill-posed Problems, John Wiley & Sons, New York (1993).

15. Groetsch, C.W., "Optimal Order of Accuracy in Vasin's Method for Differentiation of Noisy Functions," J. Optimization Theory and Applications, **74**, *373–378 (1992).*

16. Murio, D.A., "Automatic Numerical Differentiation by Discrete Mollification," J. Computational Mathematics with Applications, **13**, *381–386 (1987).*

17. Thomas, J.W., Numerical Partial Differential Equations, Springer-Verlag, New York (1995).